

## Supporting information

### Syntheses, crystal structure, electrochemistry and luminescence properties of lanthano-germanotungstates

**Table S1.** Bond lengths of Ln–O (Å) for polyanions  $[\{\text{Ln}(\mu\text{-CH}_3\text{COO})\text{GeW}_{11}\text{O}_{39}(\text{H}_2\text{O})\}_2]^{12-}$  (Ln = Pr<sup>III</sup> (**3**), Nd<sup>III</sup> (**4**) and Sm<sup>III</sup> (**5**)).

**Figure S2.** The change in the average bond lengths Ln–O (Å) in the polyanion clusters  $[\{\text{Ln}(\mu\text{-CH}_3\text{COO})\text{GeW}_{11}\text{O}_{39}(\text{H}_2\text{O})\}_2]^{12-}$  (Ln = Pr<sup>III</sup> (**3**), Nd<sup>III</sup> (**4**), Sm<sup>III</sup> (**5**), Eu<sup>III</sup> (**6**), Gd<sup>III</sup> (**7**), Tb<sup>III</sup> (**8**), Ho<sup>III</sup> (**10**), Er<sup>III</sup> (**11**), Tm<sup>III</sup> (**12**) and Yb<sup>III</sup> (**13**)) with the ionic radius of the lanthanoid.

**Figure S3.** FT-IR spectra of  $\text{Na}_3\text{K}_{10}[\text{Ln}(\text{GeW}_{11}\text{O}_{39})_2]\cdot n\text{H}_2\text{O}$  [Ln = {La<sup>III</sup> (**La-1a**), n = 27} and {Ce<sup>III</sup> (**Ce-2a**), n = 28}] POMs (recorded with KBr pellets).

**Figure S4.** FT-IR spectra of  $\text{Na}_x\text{K}_y[\{\text{Ln}(\mu\text{-CH}_3\text{COO})\text{GeW}_{11}\text{O}_{39}(\text{H}_2\text{O})\}_2]\cdot n\text{H}_2\text{O}$  [Ln = {Pr<sup>III</sup> (**Pr-3a**), x = 6, y = 6, n = 25}, {Nd<sup>III</sup> (**Nd-4a**), x = 4, y = 8, n = 22} and {Sm<sup>III</sup> (**Sm-5a**), x = 3, y = 9, n = 19}] POMs (recorded with KBr pellets).

**Figure S5.** FT-IR spectra of  $\text{Na}_3\text{K}_{10}[\text{La}(\text{GeW}_{11}\text{O}_{39})_2]\cdot 27\text{H}_2\text{O}$  (**La-1a**),  $\text{Na}_{10}[\alpha\text{-GeW}_9\text{O}_{34}]\cdot 18\text{H}_2\text{O}$  and  $\text{K}_8[\alpha\text{-GeW}_{11}\text{O}_{39}]\cdot 13\text{H}_2\text{O}$  POMs (recorded with KBr pellets).

**Figure S6.** UV/Vis spectra of (**La-1a**) – (**Yb-13a**) recorded in aqueous solution in the range of 190–800 nm.

**Figure S7.** Solid state UV/vis spectrum of (**Nd-4a**) POMs.

**Figure S8.** Solid state UV/vis spectrum of (**Sm-5a**) POMs.

**Figure S9.** Solid state UV/vis spectrum of (**Dy-9a**) POMs.

**Figure S10.** Solid state UV/vis spectrum of (**Tm-12a**) POMs.

**Figure S11.** Solid state Photoluminescence spectrum of (**Pr-3a**) POMs.

**Figure S12.** Solid state Photoluminescence spectrum of (**Ho-10a**) POMs.

**Figure S13.** Solid state Photoluminescence spectrum of (**Er-11a**) POMs.

**Figure S14.** Solid state Photoluminescence spectrum of (**Tm-12a**) POMs.

**Figure S15.** Thermogravimetric analysis curves of  $\text{Na}_3\text{K}_{10}[\text{Ln}(\text{GeW}_{11}\text{O}_{39})_2]\cdot n\text{H}_2\text{O}$  [Ln = {La<sup>III</sup> (**La-1a**), n = 27} and {Ce<sup>III</sup> (**Ce-2a**), n = 28}] POMs.

**Figure S16.** Thermogravimetric analysis curves of  $\text{Na}_x\text{K}_y[\{\text{Ln}(\mu\text{-CH}_3\text{COO})\text{GeW}_{11}\text{O}_{39}(\text{H}_2\text{O})\}_2]\cdot n\text{H}_2\text{O}$  [Ln = {Pr<sup>III</sup> (**Pr-3a**), x = 6, y = 6, n = 25},

{Nd<sup>III</sup> (**Nd-4a**), x = 4, y = 8, n = 22} and {Sm<sup>III</sup> (**Sm-5a**), x = 3, y = 9, n = 19}] POMs.

**Figure S17.** VSM Plot of magnetization (M) vs magnetic field (H) for (**La-1a**) - (**Sm-5a**) POMs at room temperature.

**Figure S18.** CVs of **Pr-3a** in 1.0 M LiCH<sub>3</sub>COO + CH<sub>3</sub>COOH / pH 4 (black), pH 5 (red) and pH 6 (blue).

**Table S19.** Cathodic peak potentials,  $E_{pc}$ , anodic peak potentials,  $E_{pa}$ , and standard midpoint redox potentials,  $E^{0'} = (E_{pa} + E_{pc})/2$ , for the W centre reduction steps of **Pr-3a** in 1.0 M LiCH<sub>3</sub>COO + CH<sub>3</sub>COOH, from pH 4 to pH 6.

**Figure S20.** CVs of **Nd-4a** in 1.0 M LiCH<sub>3</sub>COO + CH<sub>3</sub>COOH / pH 4 (black), pH 5 (red) and pH 6 (blue).

**Table S21.** Cathodic peak potentials,  $E_{pc}$ , anodic peak potentials,  $E_{pa}$ , and standard midpoint redox potentials,  $E^{0'} = (E_{pa} + E_{pc})/2$ , for the W centre reduction steps of **Nd-4a** in 1.0 M LiCH<sub>3</sub>COO + CH<sub>3</sub>COOH, from pH 4 to pH 6.

**Figure S22. (A)** CVs of **Eu-6a** in 1.0 M LiCH<sub>3</sub>COO + CH<sub>3</sub>COOH / pH 4 (black), pH 5 (red) and pH 6 (blue). **(B)** CVs of **Eu-6a** (red) and **Sm-5a** (black) in 1.0 M LiCH<sub>3</sub>COO + CH<sub>3</sub>COOH / pH 5.

**Table S23.** Cathodic peak potentials,  $E_{pc}$ , anodic peak potentials,  $E_{pa}$ , and standard midpoint redox potentials,  $E^{0'} = (E_{pa} + E_{pc})/2$ , for the W centre reduction steps of **Eu-6a** in 1.0 M LiCH<sub>3</sub>COO + CH<sub>3</sub>COOH, from pH 4 to pH 6.

**Figure S24.** CVs of **Tb-8a** in 1.0 M LiCH<sub>3</sub>COO + CH<sub>3</sub>COOH / pH 4 (black), pH 5 (red) and pH 6 (blue).

**Table S25.** Cathodic peak potentials,  $E_{pc}$ , anodic peak potentials,  $E_{pa}$ , and standard midpoint redox potentials,  $E^{0'} = (E_{pa} + E_{pc})/2$ , for the W centre reduction steps of **Tb-8a** in 1.0 M LiCH<sub>3</sub>COO + CH<sub>3</sub>COOH, from pH 4 to pH 6.

**Figure S26.** CVs of **Dy-9a** in 1.0 M LiCH<sub>3</sub>COO + CH<sub>3</sub>COOH / pH 4 (black), pH 5 (red) and pH 6 (blue).

**Table S27.** Cathodic peak potentials,  $E_{pc}$ , anodic peak potentials,  $E_{pa}$ , and standard midpoint redox potentials,  $E^{0'} = (E_{pa} + E_{pc})/2$ , for the W centre reduction steps of **Dy-9a** in 1.0 M LiCH<sub>3</sub>COO + CH<sub>3</sub>COOH, from pH 4 to pH 6.

**Figure S28.** CVs of **Ho-10a** in 1.0 M LiCH<sub>3</sub>COO + CH<sub>3</sub>COOH / pH 4 (black), pH 5 (red) and pH 6 (blue).

**Table S29.** Cathodic peak potentials,  $E_{pc}$ , anodic peak potentials,  $E_{pa}$ , and standard midpoint redox potentials,  $E^{0'} = (E_{pa} + E_{pc})/2$ , for the W centre

reduction steps of **Ho-10a** in 1.0 M LiCH<sub>3</sub>COO + CH<sub>3</sub>COOH, from pH 4 to pH 6.

**Figure S30.** CVs of **Er-11a** in 1.0 M LiCH<sub>3</sub>COO + CH<sub>3</sub>COOH / pH 4 (black), pH 5 (red) and pH 6 (blue).

**Table S31.** Cathodic peak potentials,  $E_{pc}$ , anodic peak potentials,  $E_{pa}$ , and standard midpoint redox potentials,  $E^{0'} = (E_{pa} + E_{pc})/2$ , for the W centre reduction steps of **Er-11a** in 1.0 M LiCH<sub>3</sub>COO + CH<sub>3</sub>COOH, from pH 4 to pH 6.

**Figure S32.** CVs of **Tm-12a** in 1.0 M LiCH<sub>3</sub>COO + CH<sub>3</sub>COOH / pH 4 (black), pH 5 (red) and pH 6 (blue).

**Table S33.** Cathodic peak potentials,  $E_{pc}$ , anodic peak potentials,  $E_{pa}$ , and standard midpoint redox potentials,  $E^{0'} = (E_{pa} + E_{pc})/2$ , for the W centre reduction steps of **Tm-12a** in 1.0 M LiCH<sub>3</sub>COO + CH<sub>3</sub>COOH, from pH 4 to pH 6.

**Table S1.** Bond lengths of Ln-O (Å) for polyanions [**Ln**( $\mu$ -CH<sub>3</sub>COO)GeW<sub>11</sub>O<sub>39</sub>(H<sub>2</sub>O)<sub>2</sub>]<sup>12-</sup> (Ln = Pr<sup>III</sup> (**3**), Nd<sup>III</sup> (**4**) and Sm<sup>III</sup> (**5**)).

<b>Ln<sup>III</sup></b>	<b>Pr</b>	<b>Nd</b>	<b>Sm</b>
Ln-O37	2.4204(11)	2.3835(17)	2.3805(10)
Ln-O38	2.4223(11)	2.3898(19)	2.3701(84)
Ln-O39	2.4295(11)	2.4043(18)	2.3886(90)
Ln-O40	2.3665(12)	2.3262(18)	2.3391(99)
Ln-O41	2.5128(11)	2.4998(17)	2.4535(90)
Ln-O42	2.5854(13)	2.5733(20)	2.5538(11)
Ln-O43	2.5644(11)	2.5519(17)	2.5114(89)
Ln-O44	2.5193(11)	2.5181(17)	2.4822(88)
<b>Average</b>	<b>2.48</b>	<b>2.46</b>	<b>2.44</b>

The average Ln-O bond lengths (Å) of the polyanion of **Eu<sup>III</sup>** = 2.41, **Gd<sup>III</sup>** = 2.41, **Tb<sup>III</sup>** = 2.40, **Ho<sup>III</sup>** = 2.38, **Er<sup>III</sup>** = 2.37, **Tm<sup>III</sup>** = 2.36 and **Yb<sup>III</sup>** = 2.35 as seen in the published paper *J. Solid State Chem.*, 2011, **184**, 214.

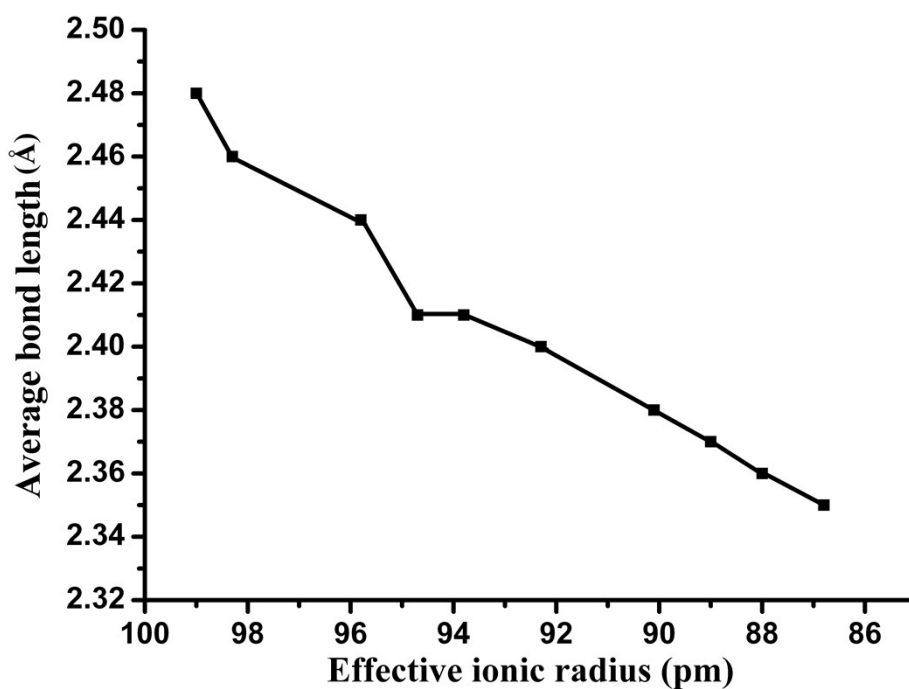


**Figure S2.** The change in the average bond lengths Ln–O (Å) in the polyanion clusters  $[\{\text{Ln}(\mu\text{-CH}_3\text{COO})\text{GeW}_{11}\text{O}_{39}(\text{H}_2\text{O})\}_2]^{12-}$  (Ln = Pr<sup>III</sup> (3), Nd<sup>III</sup> (4), Sm<sup>III</sup> (5), Eu<sup>III</sup> (6), Gd<sup>III</sup> (7), Tb<sup>III</sup> (8), Ho<sup>III</sup> (10), Er<sup>III</sup> (11), Tm<sup>III</sup> (12) and Yb<sup>III</sup> (13)) with the ionic radius of the lanthanoid.

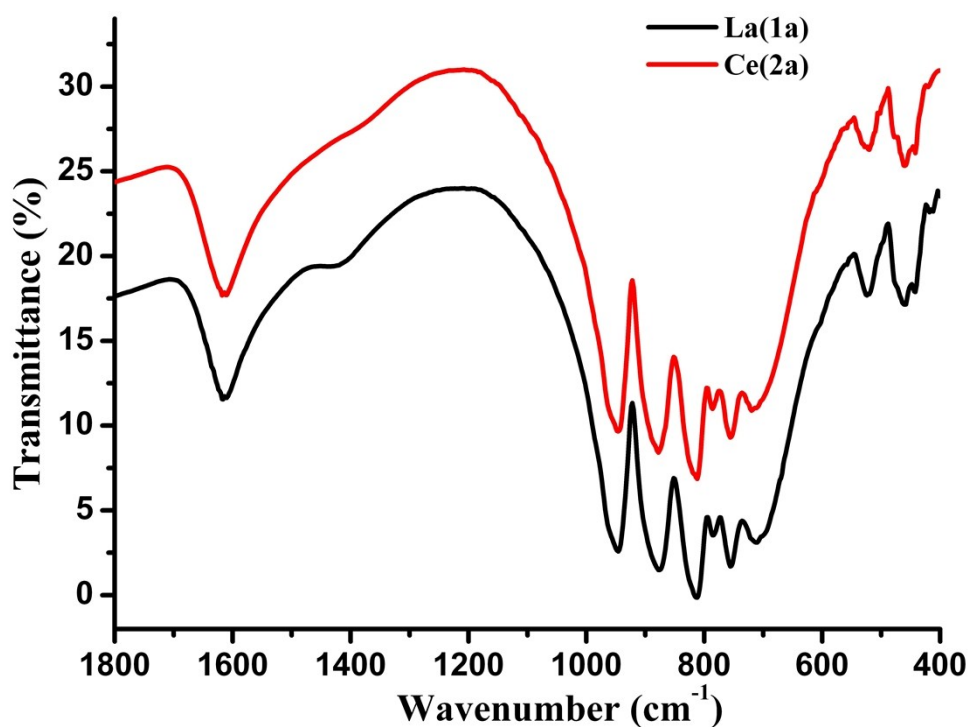


**Figure S3.** FT-IR spectra of  $\text{Na}_3\text{K}_{10}[\text{Ln}(\text{GeW}_{11}\text{O}_{39})_2] \cdot n\text{H}_2\text{O}$  [Ln = {La<sup>III</sup> (La-1a), n = 27} and {Ce<sup>III</sup> (Ce-2a), n = 28}] POMs (recorded with KBr pellets).

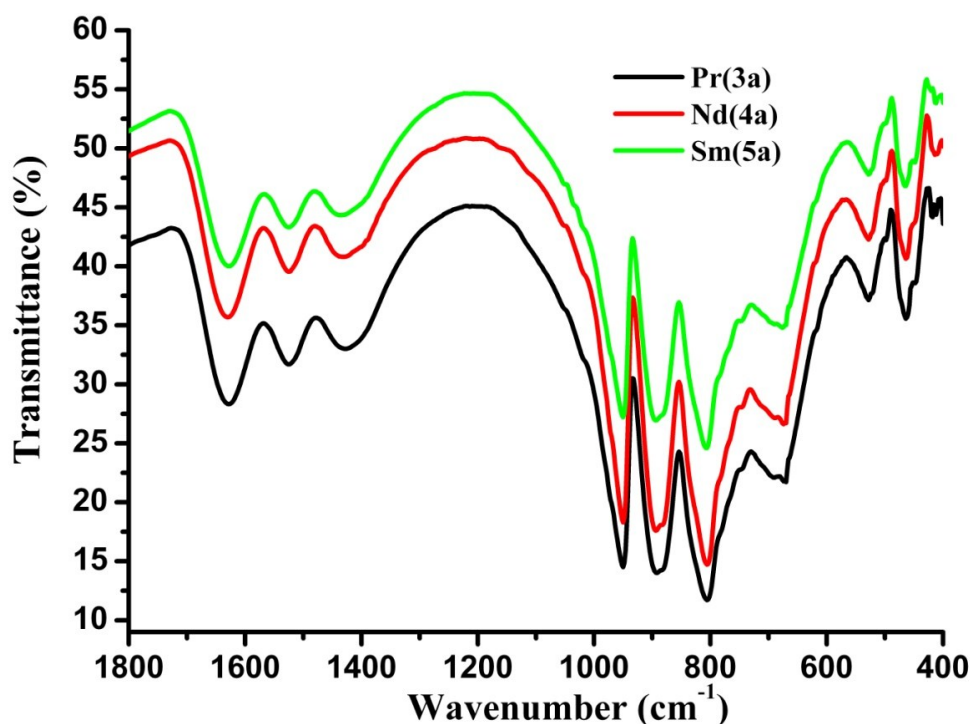


**Figure S4.** FT-IR spectra of  $\text{Na}_x\text{K}_y[\{\text{Ln}(\mu\text{-CH}_3\text{COO})\text{GeW}_{11}\text{O}_{39}(\text{H}_2\text{O})\}_2]\cdot n\text{H}_2\text{O}$  [ $\text{Ln} = \{\text{Pr}^{\text{III}}$  (**Pr-3a**),  $x = 6$ ,  $y = 6$ ,  $n = 25\}$ ,  $\{\text{Nd}^{\text{III}}$  (**Nd-4a**),  $x = 4$ ,  $y = 8$ ,  $n = 22\}$  and  $\{\text{Sm}^{\text{III}}$  (**Sm-5a**),  $x = 3$ ,  $y = 9$ ,  $n = 19\}$ ] POMs (recorded with KBr pellets).

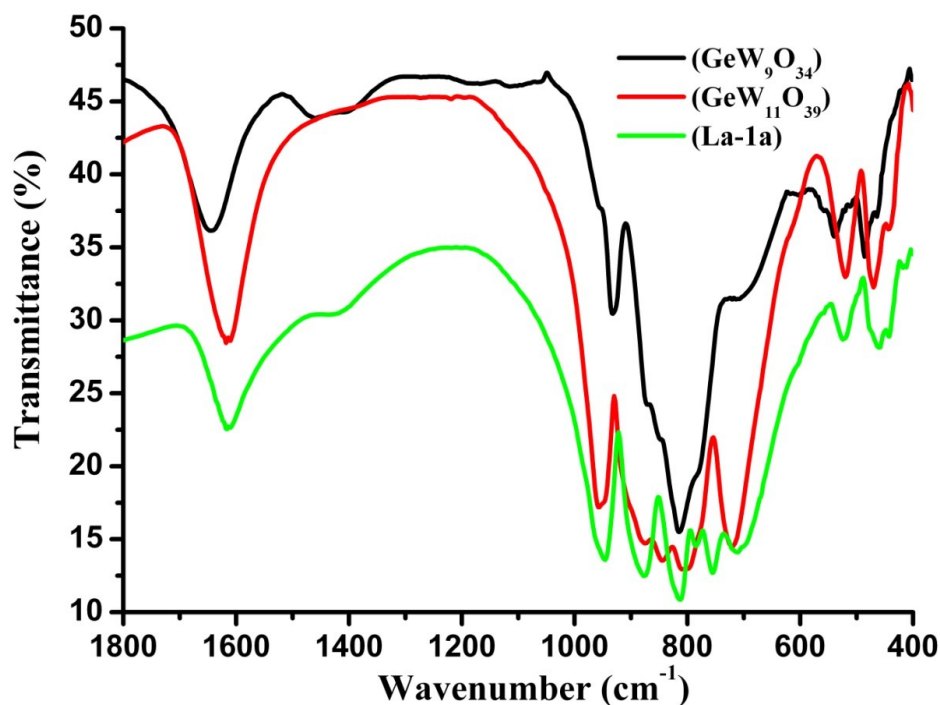


**Figure S5.** FT-IR spectra of  $\text{Na}_3\text{K}_{10}[\text{La}(\text{GeW}_{11}\text{O}_{39})_2]\cdot 27\text{H}_2\text{O}$  (**La-1a**),  $\text{Na}_{10}[\alpha\text{-GeW}_9\text{O}_{34}]\cdot 18\text{H}_2\text{O}$  and  $\text{K}_8[\alpha\text{-GeW}_{11}\text{O}_{39}]\cdot 13\text{H}_2\text{O}$  POMs (recorded with KBr pellets).

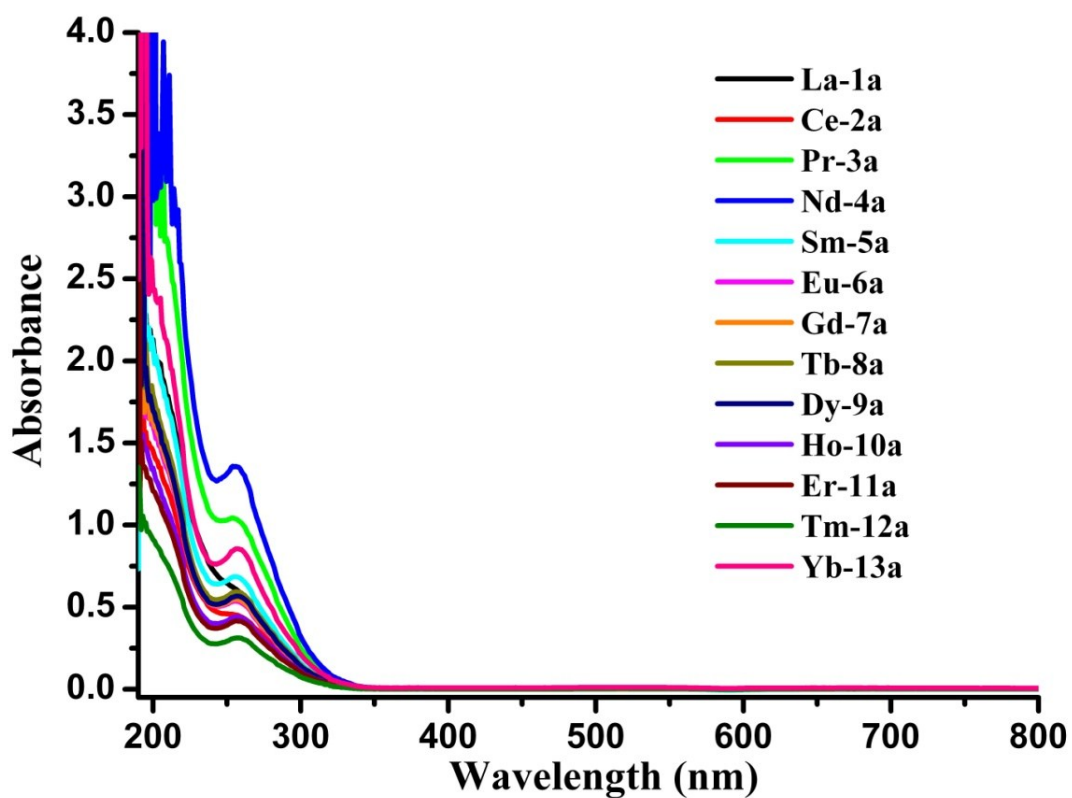


**Figure S6.** UV/Vis spectra of (La-1a) – (Yb-13a) recorded in aqueous solution in the range of 190-800 nm.

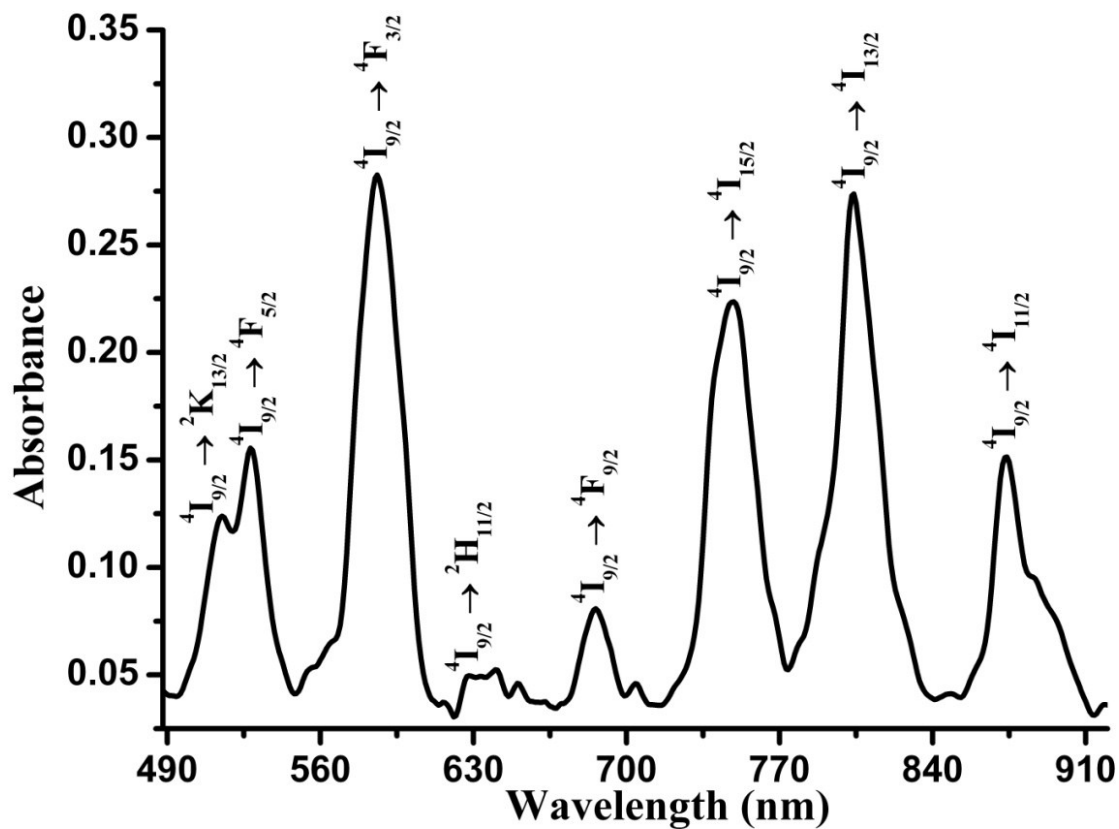


**Figure S7.** Solid state UV/vis spectrum of (Nd-4a) POMs.

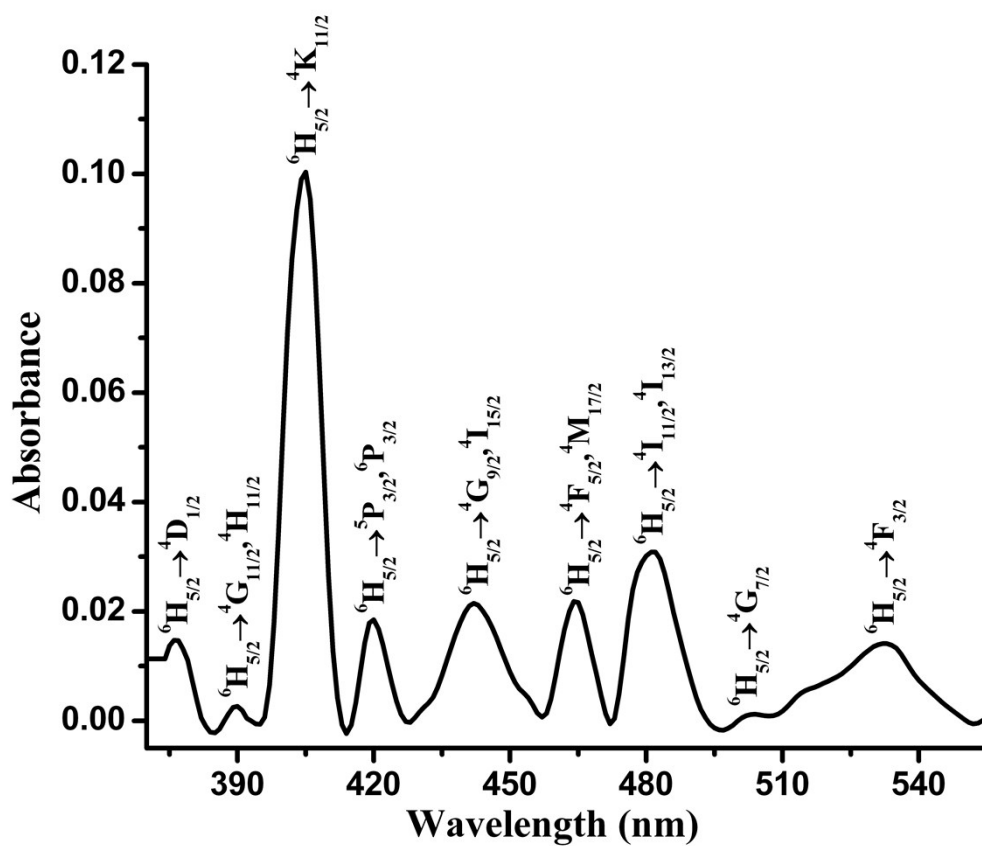


**Figure S8.** Solid state UV/vis spectrum of (**Sm-5a**) POMs.

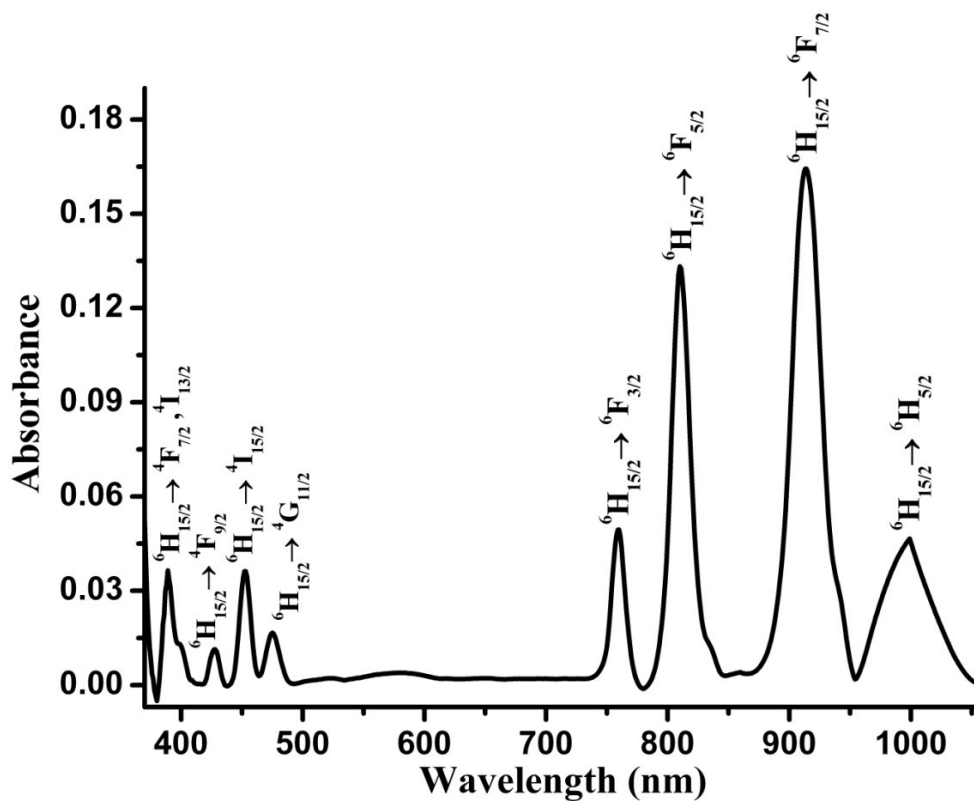


**Figure S9.** Solid state UV/vis spectrum of (**Dy-9a**) POMs.

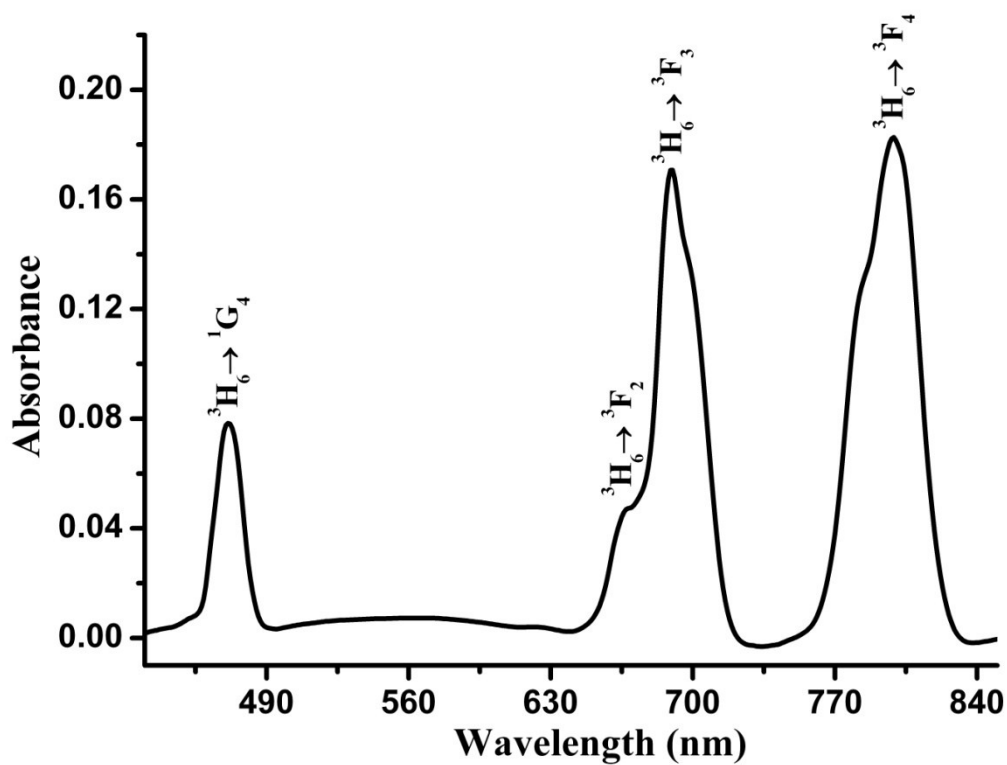


**Figure S10.** Solid state UV/vis spectrum of (Tm-12a) POMs.

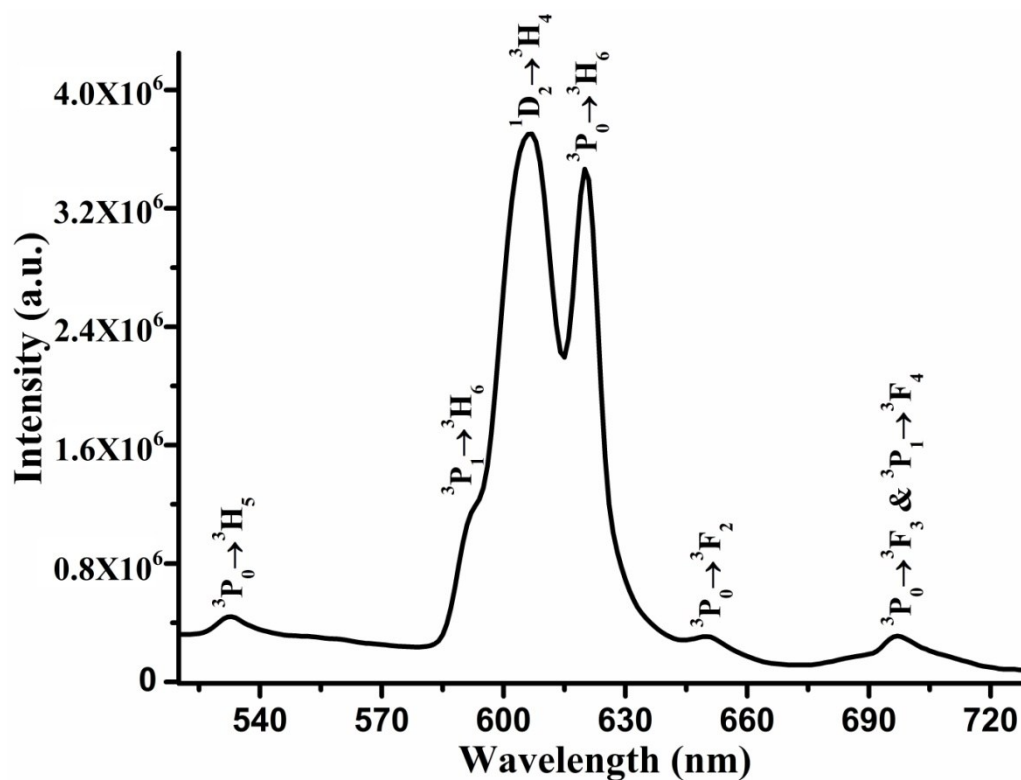


**Figure S11.** Solid state Photoluminescence spectrum of (Pr-3a) POMs.

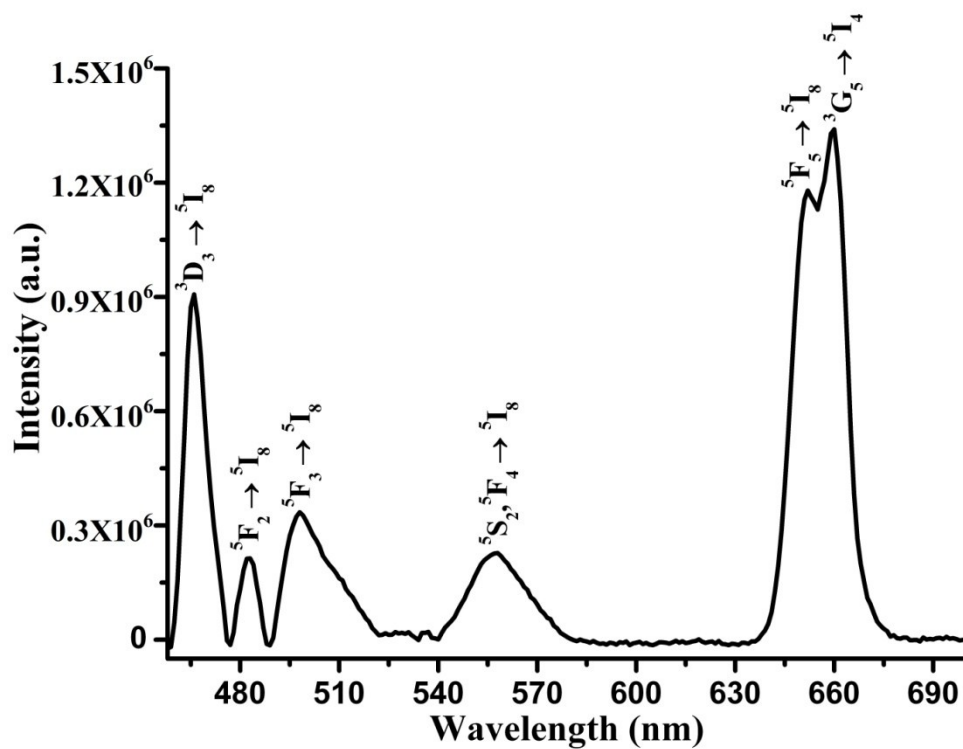


**Figure S12.** Solid state Photoluminescence spectrum of **(Ho-10a)** POMs.

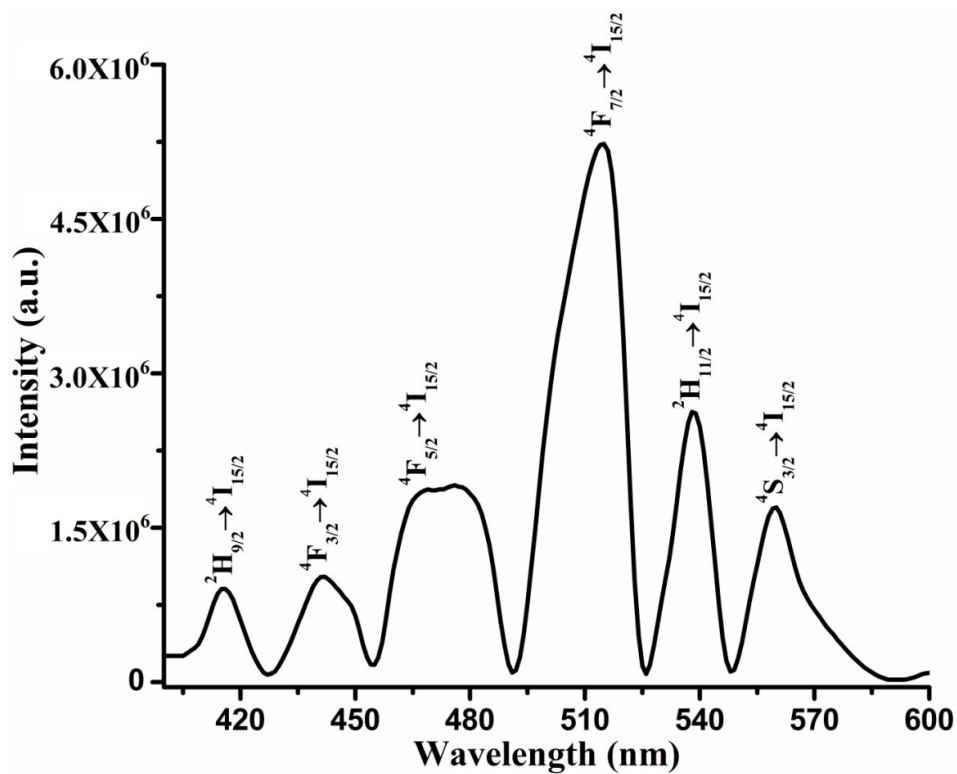


**Figure S13.** Solid state Photoluminescence spectrum of **(Er-11a)** POMs.

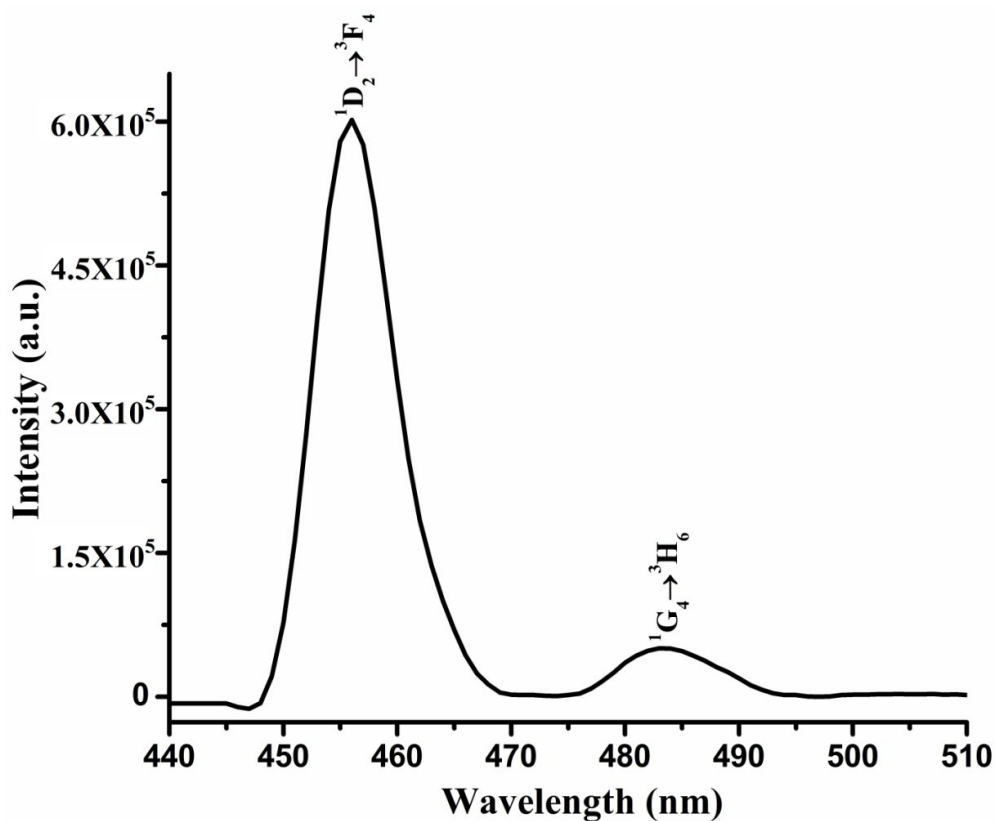


**Figure S14.** Solid state Photoluminescence spectrum of (Tm-12a) POMs.

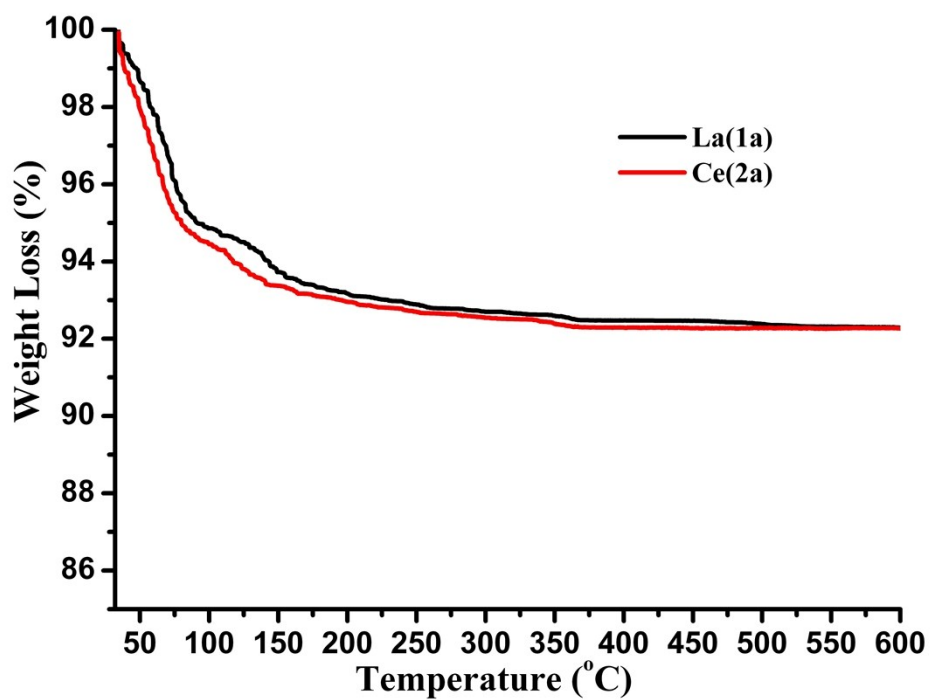


**Figure S15.** Thermogravimetric analysis curves of  $\text{Na}_3\text{K}_{10}[\text{Ln}(\text{GeW}_{11}\text{O}_{39})_2]\cdot n\text{H}_2\text{O}$  [ $\text{Ln} = \{\text{La}^{\text{III}}$  (**La-1a**),  $n = 27\}$  and  $\{\text{Ce}^{\text{III}}$  (**Ce-2a**),  $n = 28\}$ ] POMs.

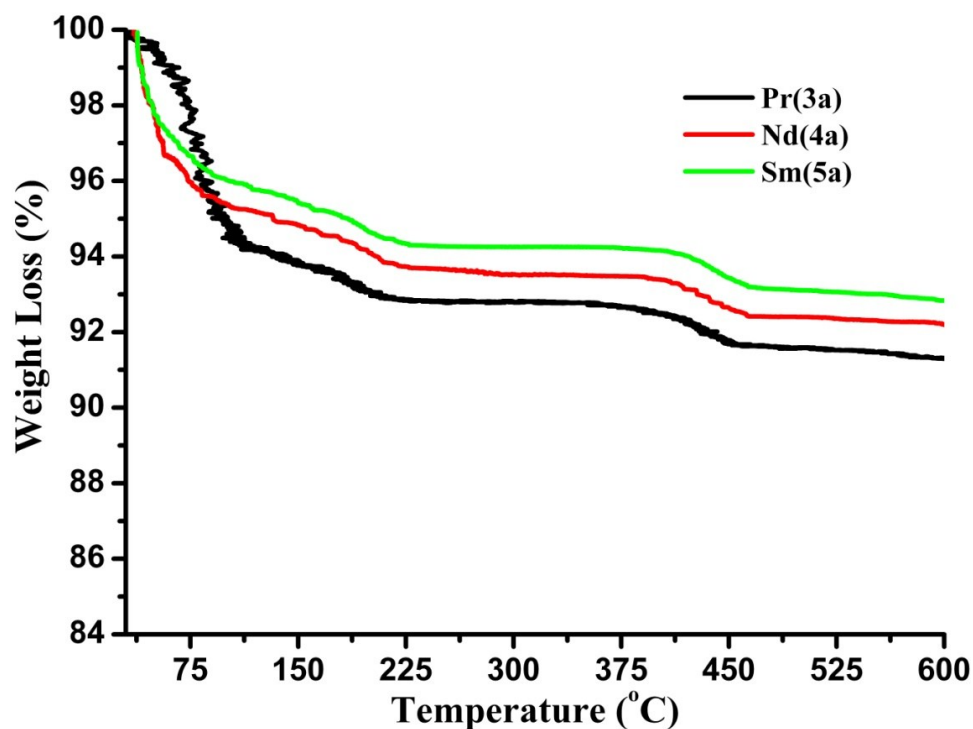


**Figure S16.** Thermogravimetric analysis curves of  $\text{Na}_x\text{K}_y[\{\text{Ln}(\mu\text{-CH}_3\text{COO})\text{GeW}_{11}\text{O}_{39}(\text{H}_2\text{O})\}_2]\cdot n\text{H}_2\text{O}$  [ $\text{Ln} = \{\text{Pr}^{\text{III}}$  (**Pr-3a**),  $x = 6$ ,  $y = 6$ ,  $n = 25\}$ ,  $\{\text{Nd}^{\text{III}}$  (**Nd-4a**),  $x = 4$ ,  $y = 8$ ,  $n = 22\}$  and  $\{\text{Sm}^{\text{III}}$  (**Sm-5a**),  $x = 3$ ,  $y = 9$ ,  $n = 19\}$ ] POMs.

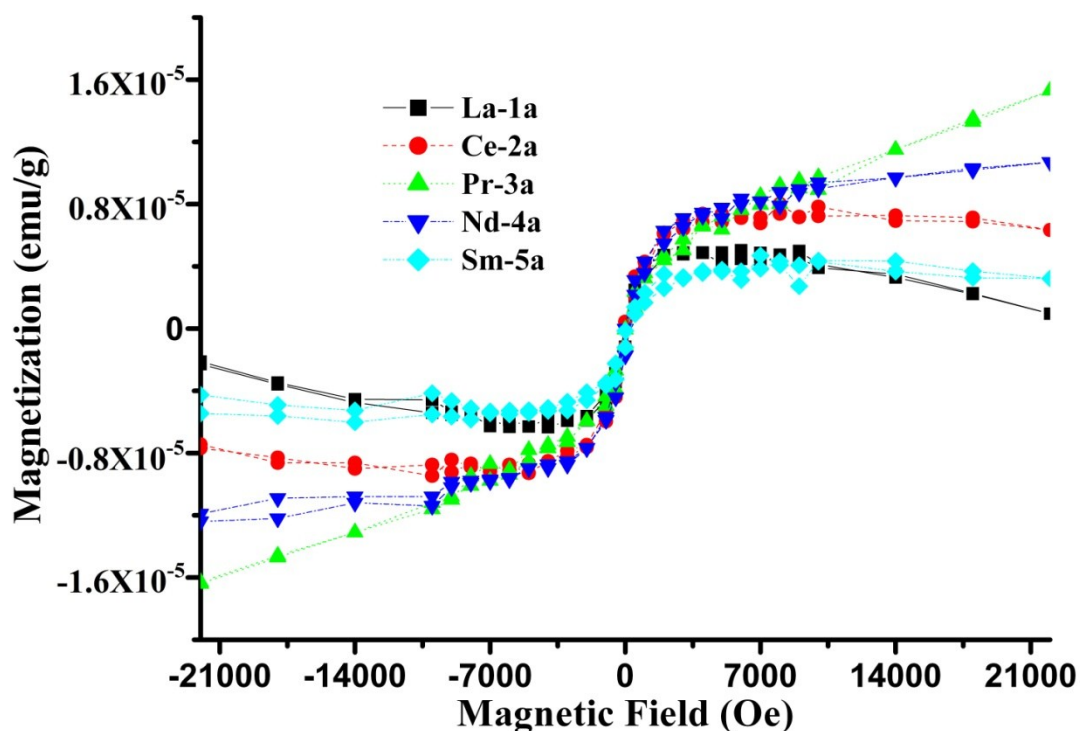


**Figure S17.** VSM Plot of magnetization (M) vs magnetic field (H) for (**La-1a**) - (**Sm-5a**) POMs at room temperature.

At pH 4, the first redox process of **Pr-3a** is not distinct from the second one. There is a single reduction peak and a partially composite oxidation process (see **fig. S18**).

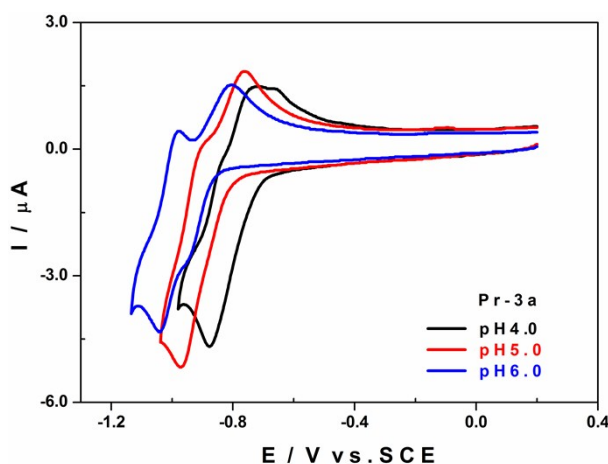


**Figure S18.** CVs of **Pr-3a** in 1.0 M LiCH<sub>3</sub>COO + CH<sub>3</sub>COOH / pH 4 (black), pH 5 (red) and pH 6 (blue). The scan starts in the direction of the negative potentials and reveals the waves attributed to the W<sup>VI</sup> centres. Scan rate: 10 mV s<sup>-1</sup>; working electrode: glassy carbon; counter electrode: Pt; reference electrode: SCE.

**Table S19.** Cathodic peak potentials,  $E_{pc}$ , anodic peak potentials,  $E_{pa}$ , and standard midpoint redox potentials,  $E^{0'} = (E_{pa} + E_{pc})/2$ , for the W centre reduction steps of **Pr-3a** in 1.0 M LiCH<sub>3</sub>COO + CH<sub>3</sub>COOH, from pH 4 to pH 6. The CVs were recorded at a scan rate of 10 mV s<sup>-1</sup>; working electrode: glassy carbon; reference electrode: SCE.

<b>Pr-3a (V vs. SCE)</b>				
pH	4.0	5.0	6.0	□ V / pH
$E_{pc1}$	-	<b>-0.880</b>	<b>-0.950</b>	-
$E_{pa1}$	-	<b>-0.760</b>	<b>-0.800</b>	-
$E_1^{0'}$	-	<b>-0.820</b>	<b>-0.875</b>	<b>-0.065</b>
$E_{pc2}$	<b>-0.880</b>	<b>-0.970</b>	<b>-1.040</b>	-

$E_{pa2}$	<b>-0.850</b>	<b>-0.920</b>	<b>-0.980</b>	-
$E_2^{0'}$	<b>-0.865</b>	<b>-0.945</b>	<b>-1.010</b>	<b>-0.070</b>

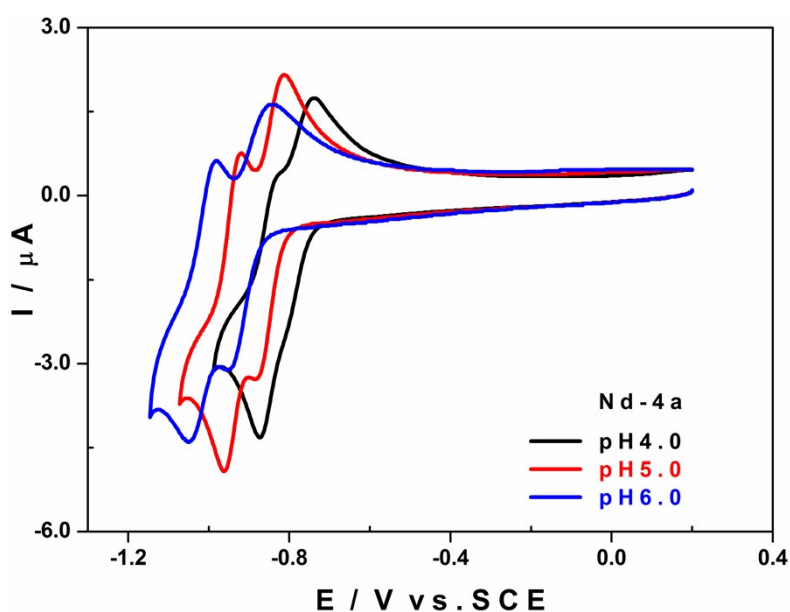


**Figure S20.** CVs of **Nd-4a** in 1.0 M  $\text{LiCH}_3\text{COO} + \text{CH}_3\text{COOH}$  / pH 4 (black), pH 5 (red) and pH 6 (blue). The scan starts in the direction of the negative potentials and reveals the waves attributed to the  $\text{W}^{\text{VI}}$  centres. Scan rate:  $10 \text{ mV s}^{-1}$ ; working electrode: glassy carbon; counter electrode: Pt; reference electrode: SCE.

**Table S21.** Cathodic peak potentials,  $E_{pc}$ , anodic peak potentials,  $E_{pa}$ , and standard midpoint redox potentials,  $E^{0'} = (E_{pa} + E_{pc})/2$ , for the W centre reduction steps of **Nd-4a** in 1.0 M  $\text{LiCH}_3\text{COO} + \text{CH}_3\text{COOH}$ , from pH 4 to pH 6. The CVs were recorded at a scan rate of  $10 \text{ mV s}^{-1}$ ; working electrode: glassy carbon; reference electrode: SCE.

Nd-4a (V vs. SCE)				
pH	4.0	5.0	6.0	□ V / pH
$E_{pc1}$	<b>-0.810</b>	<b>-0.880</b>	<b>-0.950</b>	-
$E_{pa1}$	<b>-0.740</b>	<b>-0.810</b>	<b>-0.840</b>	-
$E_1^{0'}$	<b>-0.775</b>	<b>-0.845</b>	<b>-0.895</b>	<b>-0.060</b>
$E_{pc2}$	<b>-0.870</b>	<b>-0.960</b>	<b>-1.050</b>	-
$E_{pa2}$	<b>-0.830</b>	<b>-0.920</b>	<b>-0.980</b>	-
$E_2^{0'}$	<b>-0.850</b>	<b>-0.940</b>	<b>-1.015</b>	<b>-0.080</b>

The comparison of the CVs of compounds **Eu-6a** and **Sm-5a** (see **fig. S22B**) reveals that the former has more intense reduction waves than the latter, despite the fact that both were obtained in the same experimental conditions (scan rate, concentration, working electrode, ...). This behaviour is similar to that described in one of our previous studies<sup>1</sup>, where we showed that the  $\text{Eu}^{\text{III}}$  centre was reduced in the same potential range as the  $\text{W}^{\text{VI}}$  centres, resulting in a higher reduction current for **Eu-6a**.

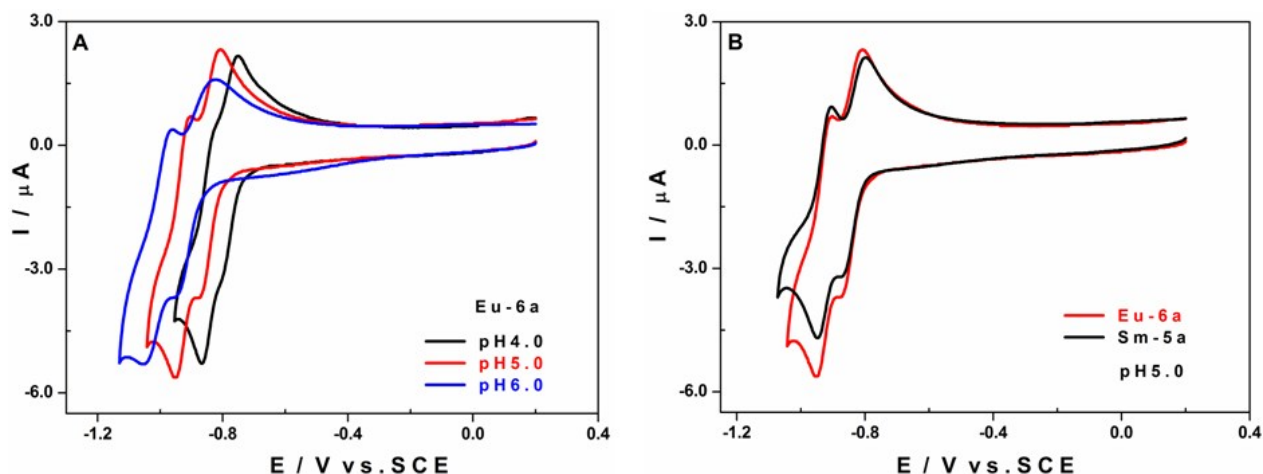


**Figure S22.** (A) CVs of **Eu-6a** in 1.0 M  $\text{LiCH}_3\text{COO} + \text{CH}_3\text{COOH}$  / pH 4 (black), pH 5 (red) and pH 6 (blue). (B) CVs of **Eu-6a** (red) and **Sm-5a** (black) in 1.0 M  $\text{LiCH}_3\text{COO} + \text{CH}_3\text{COOH}$  / pH 5. The scan starts in the direction of the negative potentials and reveals the waves attributed to the  $\text{W}^{\text{VI}}$  centres. Scan

rate: 10 mV s<sup>-1</sup>; working electrode: glassy carbon; counter electrode: Pt; reference electrode: SCE.

**Table S23.** Cathodic peak potentials,  $E_{pc}$ , anodic peak potentials,  $E_{pa}$ , and standard midpoint redox potentials,  $E^{0'} = (E_{pa} + E_{pc})/2$ , for the W centre reduction steps of **Eu-6a** in 1.0 M LiCH<sub>3</sub>COO + CH<sub>3</sub>COOH, from pH 4 to pH 6. The CVs were recorded at a scan rate of 10 mV s<sup>-1</sup>; working electrode: glassy carbon; reference electrode: SCE.

<b>Eu-6a (V vs. SCE)</b>				
pH	4.0	5.0	6.0	□V / pH
$E_{pc1}$	<b>-0.790</b>	<b>-0.880</b>	<b>-0.950</b>	-
$E_{pa1}$	<b>-0.750</b>	<b>-0.810</b>	<b>-0.820</b>	-
$E_1^{0'}$	<b>-0.770</b>	<b>-0.845</b>	<b>-0.885</b>	<b>-0.060</b>
$E_{pc2}$	<b>-0.870</b>	<b>-0.950</b>	<b>-1.050</b>	-
$E_{pa2}$	<b>-0.830</b>	<b>-0.900</b>	<b>-0.960</b>	-
$E_2^{0'}$	<b>-0.850</b>	<b>-0.930</b>	<b>-1.005</b>	<b>-0.080</b>

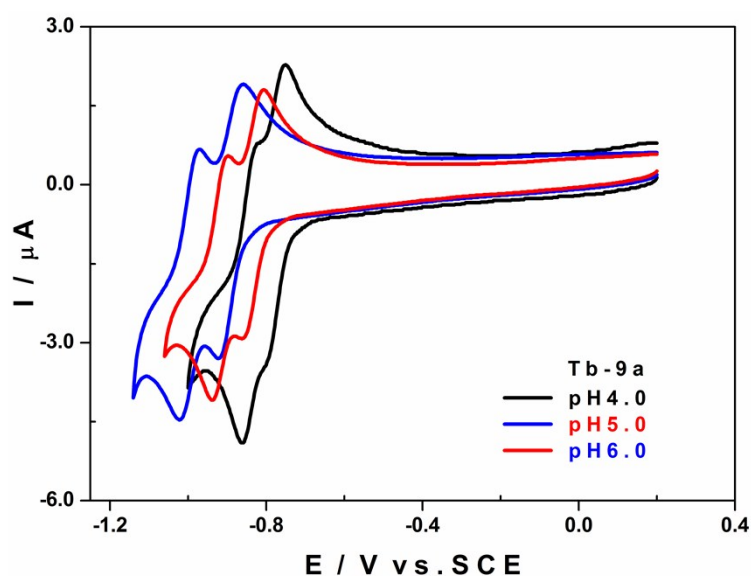


**Figure S24.** CVs of **Tb-8a** in 1.0 M LiCH<sub>3</sub>COO + CH<sub>3</sub>COOH / pH 4 (black), pH 5 (red) and pH 6 (blue). The scan starts in the direction of the negative potentials and reveals the waves attributed to the W<sup>VI</sup> centres. Scan rate: 10 mV s<sup>-1</sup>; working electrode: glassy carbon; counter electrode: Pt; reference electrode: SCE.

**Table S25.** Cathodic peak potentials,  $E_{pc}$ , anodic peak potentials,  $E_{pa}$ , and standard midpoint redox potentials,  $E^{0'} = (E_{pa} + E_{pc})/2$ , for the W centre reduction steps of **Tb-8a** in 1.0 M LiCH<sub>3</sub>COO + CH<sub>3</sub>COOH, from pH 4 to pH 6. The CVs were recorded at a scan rate of 10 mV s<sup>-1</sup>; working electrode: glassy carbon; reference electrode: SCE.

<b>Tb-8a</b> (V vs. SCE)				
pH	4.0	5.0	6.0	□ V / pH
$E_{pc1}$	<b>-0.800</b>	<b>-0.860</b>	<b>-0.920</b>	-
$E_{pa1}$	<b>-0.750</b>	<b>-0.810</b>	<b>-0.860</b>	-
$E_1^{0'}$	<b>-0.780</b>	<b>-0.835</b>	<b>-0.890</b>	<b>-0.055</b>
$E_{pc2}$	<b>-0.860</b>	<b>-0.940</b>	<b>-1.020</b>	-
$E_{pa2}$	<b>-0.820</b>	<b>-0.900</b>	<b>-0.970</b>	-
$E_2^{0'}$	<b>-0.840</b>	<b>-0.920</b>	<b>-0.995</b>	<b>-0.080</b>

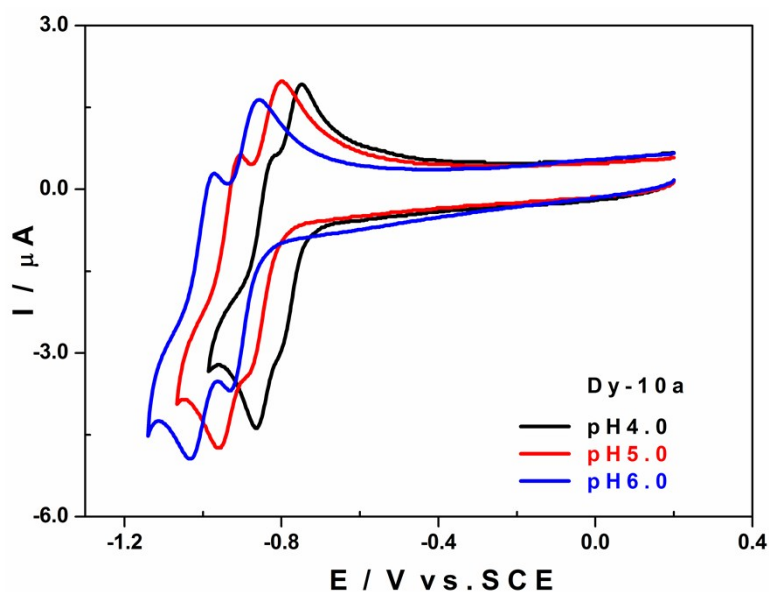


**Figure S26.** CVs of **Dy-9a** in 1.0 M LiCH<sub>3</sub>COO + CH<sub>3</sub>COOH / pH 4 (black), pH 5 (red) and pH 6 (blue). The scan starts in the direction of the negative potentials and reveals the waves attributed to the W<sup>VI</sup> centres. Scan rate: 10 mV s<sup>-1</sup>; working electrode: glassy carbon; counter electrode: Pt; reference electrode: SCE.

**Table S27.** Cathodic peak potentials,  $E_{pc}$ , anodic peak potentials,  $E_{pa}$ , and standard midpoint redox potentials,  $E^{0'} = (E_{pa} + E_{pc})/2$ , for the W centre reduction steps of **Dy-9a** in 1.0 M LiCH<sub>3</sub>COO + CH<sub>3</sub>COOH, from pH 4 to pH 6. The CVs were recorded at a scan rate of 10 mV s<sup>-1</sup>; working electrode: glassy carbon; reference electrode: SCE.

<b>Dy-9a (V vs. SCE)</b>				
pH	4.0	5.0	6.0	□ V / pH
$E_{pc1}$	<b>-0.800</b>	<b>-0.880</b>	<b>-0.930</b>	-
$E_{pa1}$	<b>-0.750</b>	<b>-0.800</b>	<b>-0.860</b>	-
$E_1^{0\prime}$	<b>-0.775</b>	<b>-0.840</b>	<b>-0.895</b>	<b>-0.060</b>
$E_{pc2}$	<b>-0.860</b>	<b>-0.960</b>	<b>-1.030</b>	-
$E_{pa2}$	<b>-0.820</b>	<b>-0.900</b>	<b>-0.970</b>	-
$E_2^{0\prime}$	<b>-0.840</b>	<b>-0.930</b>	<b>-1.000</b>	<b>-0.080</b>

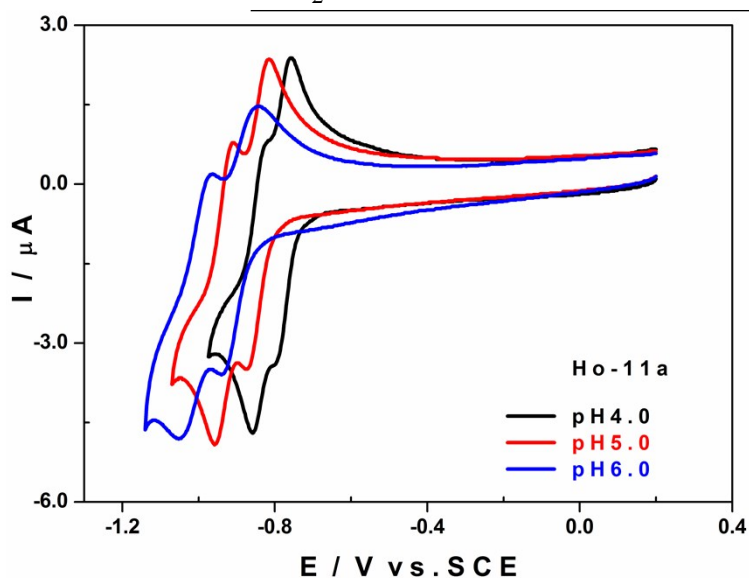


**Figure S28.** CVs of **Ho-10a** in 1.0 M LiCH<sub>3</sub>COO + CH<sub>3</sub>COOH / pH 4 (black), pH 5 (red) and pH 6 (blue). The scan starts in the direction of the negative potentials and reveals the waves attributed to the W<sup>VI</sup> centres. Scan rate: 10 mV s<sup>-1</sup>; working electrode: glassy carbon; counter electrode: Pt; reference electrode: SCE.

**Table S29.** Cathodic peak potentials,  $E_{pc}$ , anodic peak potentials,  $E_{pa}$ , and standard midpoint redox potentials,  $E^{0\prime} = (E_{pa} + E_{pc})/2$ , for the W centre reduction steps of **Ho-10a** in 1.0 M LiCH<sub>3</sub>COO + CH<sub>3</sub>COOH, from pH 4 to pH 6. The CVs were recorded at a scan rate of 10 mV s<sup>-1</sup>; working electrode: glassy carbon; reference electrode: SCE.

<b>Ho-10a (V vs. SCE)</b>
---------------------------

pH	4.0	5.0	6.0	□ V / pH
$E_{pc1}$	<b>-0.800</b>	<b>-0.870</b>	<b>-0.940</b>	-
$E_{pa1}$	<b>-0.760</b>	<b>-0.810</b>	<b>-0.840</b>	-
$E_1^{0'}$	<b>-0.780</b>	<b>-0.840</b>	<b>-0.890</b>	<b>-0.055</b>
$E_{pc2}$	<b>-0.860</b>	<b>-0.960</b>	<b>-1.050</b>	-
$E_{pa2}$	<b>-0.830</b>	<b>-0.910</b>	<b>-0.960</b>	-
$E_2^{0'}$	<b>-0.845</b>	<b>-0.935</b>	<b>-1.005</b>	<b>-0.080</b>

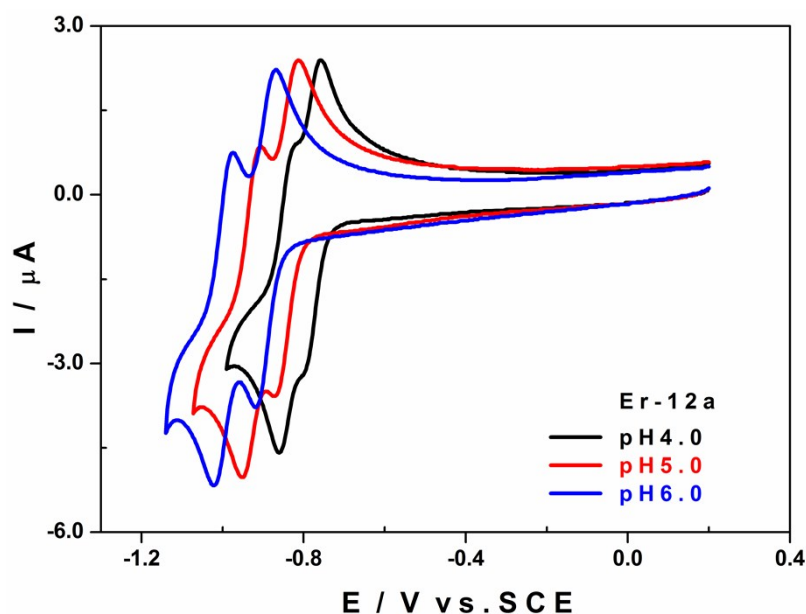


**Figure S30.** CVs of **Er-11a** in 1.0 M  $\text{LiCH}_3\text{COO} + \text{CH}_3\text{COOH}$  / pH 4 (black), pH 5 (red) and pH 6 (blue). The scan starts in the direction of the negative potentials and reveals the waves attributed to the  $\text{W}^{\text{VI}}$  centres. Scan rate:  $10 \text{ mV s}^{-1}$ ; working electrode: glassy carbon; counter electrode: Pt; reference electrode: SCE.

**Table S31.** Cathodic peak potentials,  $E_{pc}$ , anodic peak potentials,  $E_{pa}$ , and standard midpoint redox potentials,  $E^{0'} = (E_{pa} + E_{pc})/2$ , for the W centre reduction steps of **Er-11a** in 1.0 M  $\text{LiCH}_3\text{COO} + \text{CH}_3\text{COOH}$ , from pH 4 to pH 6. The CVs were recorded at a scan rate of  $10 \text{ mV s}^{-1}$ ; working electrode: glassy carbon; reference electrode: SCE.

Er-11a (V vs. SCE)				
pH	4.0	5.0	6.0	□ V / pH
$E_{pc1}$	-0.800	-0.870	-0.920	-
$E_{pa1}$	-0.760	-0.810	-0.870	-
$E_1^{0'}$	-0.780	-0.840	-0.895	-0.060
$E_{pc2}$	-0.860	-0.950	-1.020	-
$E_{pa2}$	-0.820	-0.910	-0.970	-
$E_2^{0'}$	-0.840	-0.930	-0.995	-0.080

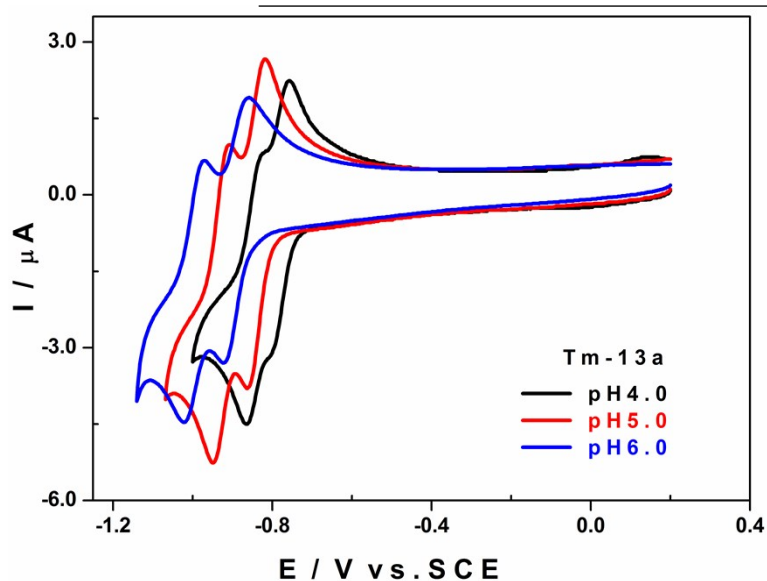


**Figure S32.** CVs of **Tm-12a** in 1.0 M LiCH<sub>3</sub>COO + CH<sub>3</sub>COOH / pH 4 (black), pH 5 (red) and pH 6 (blue). The scan starts in the direction of the negative potentials and reveals the waves attributed to the W<sup>VI</sup> centres. Scan rate: 10 mV s<sup>-1</sup>; working electrode: glassy carbon; counter electrode: Pt; reference electrode: SCE.

**Table S33.** Cathodic peak potentials,  $E_{pc}$ , anodic peak potentials,  $E_{pa}$ , and standard midpoint redox potentials,  $E^{0'} = (E_{pa} + E_{pc})/2$ , for the W centre reduction steps of **Tm-12a** in 1.0 M LiCH<sub>3</sub>COO + CH<sub>3</sub>COOH, from pH 4 to pH 6. The CVs were recorded at a scan rate of 10 mV s<sup>-1</sup>; working electrode: glassy carbon; reference electrode: SCE.

<b>Tm-12a (V vs. SCE)</b>				
pH	4.0	5.0	6.0	□ V / pH
$E_{pc1}$	<b>-0.800</b>	<b>-0.860</b>	<b>-0.920</b>	-
$E_{pa1}$	<b>-0.760</b>	<b>-0.920</b>	<b>-0.860</b>	-
$E_1^{0'}$	<b>-0.780</b>	<b>-0.890</b>	<b>-0.890</b>	<b>-0.055</b>
$E_{pc2}$	<b>-0.860</b>	<b>-0.950</b>	<b>-1.020</b>	-
$E_{pa2}$	<b>-0.830</b>	<b>-0.910</b>	<b>-0.970</b>	-
$E_2^{0'}$	<b>-0.845</b>	<b>-0.930</b>	<b>-0.995</b>	<b>-0.075</b>

## References

- 
- 1 R. Gupta, M. K. Saini, F. Doungmene, P. de Oliveira, F. Hussain, *Dalton Trans.*, 2014, **43**, 8290.